Control-based continuation for investigating nonlinear experiments

— Source link ↗

David A W Barton, Brian P. Mann, Stephen G. Burrow

Institutions: Duke University, University of Bristol

Related papers:

- Control based bifurcation analysis for experiments

- Numerical Continuation in a Physical Experiment: Investigation of a Nonlinear Energy Harvester

- Experimental Continuation of Periodic Orbits through a Fold

- Experimental bifurcation analysis of an impact oscillator—Tuning a non-invasive control scheme

- Control-based continuation of unstable periodic orbits

Barton, DAW., Mann, Bria, P., & Burrow, SG. (2010). *Control-based continuation for investigating nonlinear experiments*. http://hdl.handle.net/1983/1648

Early version, also known as pre-print

University of Bristol - Explore Bristol Research

General rights

Control-based continuation for investigating nonlinear experiments

David A.W. Barton,[*] Brian P. Mann[†] and Stephen G. Burrow[‡]

10th May 2010

Abstract

This paper presents a systematic experimental study of two one-degree-of-freedom nonlinear devices using the newly introduced control-based continuation method by Sieber and Krauskopf [Nonlinear Dynamics 2008]. By considering hardening, softening and bistable spring characteristics we demonstrate the versitility and power of the control-based continuation method for investigating nonlinear experiments. We show that, using this method, it is possible to track the stable orbits of the devices through a saddle-node bifurcation (fold) where they lose stability and continue them up to the resonance peak where they undergo a second saddle-node bifurcation. For the bistable case, a bifurcation diagram is produced that is strongly reminiscent of the bifurcation diagram produced using the classical harmonic balance solution. A detailed introduction to general continuation methods is included to enable implementation by other experimentalists.

1   Introduction

In the study of nonlinear devices it is commonplace to compute bifurcation diagrams which divide parameter space into regions of qualitatively different dynamics [Breakspear et al., 2006, Krauskopf, 2005, Stépán, 2001], e.g., transitions from a single attractor to multiple attractors. There are a variety of methods for computing bifurcation diagrams, from the simplistic, e.g., direct numerical simulation, to the more sophisticated, e.g., perturbation methods [Nayfeh, 2000] or numerical continuation [Krauskopf et al., 2007]. The common requirement for all these techniques an accurate mathematical model of the nonlinear device, which in some circumstances prevents the usefulness of the bifurcation studies, e.g., when parameter uncertainty can alter the results.

Sieber and Krauskopf [2008] recently introduced an approach which obviates the need for an accurate mathematical model, but it was still able to determine bifurcation diagrams for a nonlinear device. In particular, the authors were able to directly compute the bifurcations diagrams directly from a physical experiment, thus alleviating the need for a mathematical model. Their method, the so-called control-based continuation, is an extension of numerical continuation to a feedback-controlled experiment. (Feedback control is required to stabilise the nonlinear device in the vicinity of a bifurcation.) Much like numerical continuation offers significant advantages over direct numerical simulation by tracking stability boundaries, control-based continuation offers significant advantages over running an uncontrolled experiment. Sieber et al. [2008] provided the first experimental demonstration of this method by tracking a branch of periodic spin-solutions for a parametrically excited pendulum that underwent a saddle-node bifurcation.

In this paper, we expand on the preliminary work by Barton and Burrow [2009] and present a systematic investigation of control-based continuation applied to two nonlinear energy harvesting devices [Barton et al., 2010, Stanton et al., 2010], which are designed to convert ambient vibrations into usable power. Both devices

[*]Email: david.barton@bristol.ac.uk. Address: Department of Engineering Mathematics, University of Bristol, UK.

[†]Email: brian.mann@duke.edu. Address: Mechanical Engineering and Materials Science, Duke University, USA.

[‡]Email: stephen.burrow@bristol.ac.uk. Address: Department of Aerospace Engineering, University of Bristol, UK.

are based around cantilever beams with tip-mounted magnets, reminisant of the experimental set-up of Moon and Holmes [1979]. Depending on the particular configuration, the energy harvesters can exhibit hardening, softening or bistable spring characteristics; this is done to broaden their frequency spectrum [Mann and Owens, 2010, Mann and Sims, 2009, Stanton et al., 2009, Triplett and Quinn, 2009].

The concept of generating a bifurcation diagram directly from an experiment is not a new one; the simplest method is simply to sweep a parameter of interest (e.g., excitation frequency) and measure the corresponding response. The problem with this is that only stable behaviour is found; the unstable/saddle-type solutions, which act as separatrices (in phase-space) between different attractors, are not included. Furthermore, if there exist multiple or coexisting attractors, the experimentalist may be unable to switch between them at will. In an effort to overcome these problems, several methods built around numerical continuation have been suggested. Misra et al. [2008] consider the problem of tapping-mode atomic force microscopy and used the so-called OGY control [Ott et al., 1990] in order to continue periodic orbits through a saddle-node bifurcation. Siettos et al. [2004] described a simpler scheme with a feedback controller to stabilise an equilibrium of a particular system in conjunction with a coarse-grained bifurcation problem. So far, only control-based continuation [Sieber and Krauskopf, 2008] has been employed successfully in an experiment.

In section 2 we present the mathematical details behind numerical continuation and describe how it is combined with a control-strategy to enable its use in a physical experiment. Section 3 contains the details of the experimental set-up used within this paper and a description of the nonlinear energy harvesters investigated. We show the results from the control-based continuation in section 4 systematically applied to the energy harvesters in hardening, softening and bistable regimes. Concluding remarks and directions for future research are then given in section 5.

2 Methodology

In this section we describe control-based continuation and how it is used to generate bifurcation diagrams of an experiment without the use of a mathematical model. Here, and throughout the remainder of this paper, we adopt the convention of referring to a periodic motion of an experiment (whether stable or unstable) as a *solution* of the experiment.

There are two principal elements to control-based continuation:

Pseudo-arclength continuation Pseudo-arclength continuation is a means for tracing out solution branches of an arbitrary nonlinear function with respect to the system parameters. By extending the nonlinear function of interest with the pseudo-arclength equation, it is possible to trace out a branch in a predictor-corrector fashion through a fold or saddle-node bifurcation regardless of the stability properties of the solution.

Control strategy The purpose of the control strategy is to enable the definition of a suitable nonlinear function for use in pseudo-arclength continuation; since it is not possible to set the state of the experiment directly, a feedback controller must be used to set the state indirectly. Furthermore, a feedback controller is necessary for ensuring continuous and stable behaviour of the experiment even when operating in the vicinity of an unstable solution.

These two elements are described in detail below.

2.1 Pseudo-arclength continuation

The numerical methods underpinning pseudo-arclength continuation are well established and documented in the literature. For an introduction see, for example, Doedel et al. [1991a,b] or Seydel [2010]. In its most basic form, pseudo-arclength continuation is used to trace out solution branches of nonlinear equations of the form

$$f(x, \lambda) = 0, \qquad f : \mathbb{R}^n \times \mathbb{R}^p \to \mathbb{R}^n, \tag{1}$$
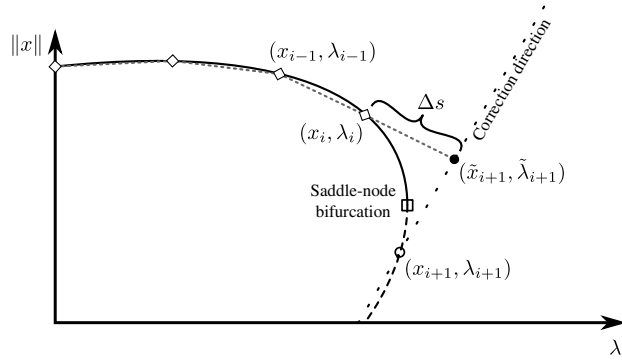
Figure 1: Graphical illustration of pseudo-arclength continuation. The solutions are computed sequentially in a predictor-corrector manner and labelled (x_i, λ_i) for $i = 1, 2, \dots$. The diamonds ($\diamond$) represent previously computed solutions along the branch, the filled circle ($\bullet$) represents the predicted solution (see (3)), and the open circle ($\circ$) represents the corrected solution.

where f is twice continuously differentiable and λ is a vector of parameters. A common example is the continuation of equilibria of a system of ordinary differential equations where x is the *state* of the system. Here f will be defined by the experiment; precise details to follow in the next section. The local existence of solution branches parameterized by λ, i.e., $x = x(\lambda)$, is generically guaranteed by the implicit function theorem. However, the conditions of implicit function theorem are not satisfied at a fold or saddle-node bifurcation where two orbits, typically one stable and one unstable, coalesce. In order to track around/through a fold, pseudo-arclength continuation reparameterizes the branch of solutions with respect to an arclength-like quantity that is defined through the pseudo-arclength equation

$$(x_i')^T (x_{i+1} - x_i) + (\lambda_i')^T (\lambda_{i+1} - \lambda_i) = \Delta s, \tag{2}$$

where the subscripts denote sequential points along the branch, the primes $()'$ denote the local tangent with respect to the arclength, Δ is a scaling parameter and s is the step size. (This is a computationally efficient approximation of the true arclength [Doedel et al., 1991a].) Geometrically, the pseudo-arclength equation constrains the correction direction to be normal to the tangent of the previous solution point (see figure 1). Thus, by forming an extended system of (1) and (2) it is possible to trace out branches of solutions parameterized by s, i.e., $x = x(s)$ and $\lambda = \lambda(s)$, which pass through folds.

Continuation of the extended system proceeds stepwise in a predictor-corrector fashion from an initial set of solution points. The procedure for this process is:

1. A predicted solution is extrapolated from the previous point in the direction of its local tangent; in this paper we use the secant approximation

$$\begin{aligned}
\tilde{x}_{i+1} &= x_i + \Delta(x_i - x_{i-1}), \\
\tilde{\lambda}_{i+1} &= \lambda_i + \Delta(\lambda_i - \lambda_{i-1}),
\end{aligned} \tag{3}$$

where Δ is a scaling parameter. For robustness it may be appropriate to use a least-squares fit through several previous points to avoid badly approximated tangents due to noise. Higher-order polynomial predictors may also be used [Seydel, 2010], however, they are rarely used in practice.

The scaling parameter Δ determines the growth of the step size as the continuation progresses. Here we choose $\Delta = 1.2$ and place an empirically determined upper bound on the maximum step size. Should the following correction step fail for any reason (e.g., non-convergence of the nonlinear root finder), Δ is set to -0.5, that is an interpolation step is performed between the previous two points before continuing. (After a successful interpolation step, the step size is approximately half its previous value.)

2. The predicted solution $(\tilde{x}_{i+1}, \tilde{\lambda}_{i+1})$ is used as an initial guess for a nonlinear root finder applied to the extended system of (1) and (2); both the values of x and λ are corrected.

3

In this paper, a Newton iteration with a Broyden update and a damping step is used as the nonlinear root finder. The Newton step is given by

$$
\begin{bmatrix} x_{i+1}^{(j+1)} \\ \lambda_{i+1}^{(j+1)} \end{bmatrix} = \begin{bmatrix} x_{i+1}^{(j)} \\ \lambda_{i+1}^{(j)} \end{bmatrix} - J^{-1} \begin{bmatrix} f(x_{i+1}^{(j)}, \lambda_{i+1}^{(j)}) \\ (x_i')^T (x_{i+1}^{(j)} - x_i) + (\lambda_i')^T (\lambda_{i+1}^{(j)} - \lambda_i) - \Delta s \end{bmatrix},
$$

where j is the current iteration number and J is the Jacobian of partial derivatives of the extended system. The Jacobian is approximated using finite differences. Since each evaluation of the extended system requires measurements from the physical experiment, it is imperative to minimise the number of function evaluations needed. Consequently, the Broyden update applies a rank-one update to the Jacobian after each iteration instead of recalculating it entirely [Eyert, 1996]. The purpose of the damping step is to try to ensure that the norm of the value of the extended system does not increase (i.e., the iteration converges towards zero monotonically). If it is found that the norm has increased then the update to the values of x and λ is halved and the extended system is evaluated again.

With pseudo-arclength continuation defined in generality for an arbitrary nonlinear function f all that remains is to specify how f can be defined through an experiment.

2.2 Control strategy

Unlike in model-based numerical continuation, where the state of a system can be set arbitrarily, the state of an experiment cannot be chosen at will without considerable difficulty, if at all. Thus, the purpose of the control strategy within control-based continuation is to provide a mechanism for setting the state and simultaneously ensuring that the system remains stable even when operating around an unstable solution.

In this paper, we exclusively consider single degree-of-freedom experiments that are periodically forced. As such, we employ a linear proportional-derivative (PD) controller with fixed gains; the control action is super-imposed on the forcing signal $\Gamma(t)$ to give a new forcing signal $\hat{\Gamma}(t)$ defined as

$$
\hat{\Gamma}(t) = \Gamma(t) + K_p(x^*(t) - x(t)) + K_d(\dot{x}^*(t) - \dot{x}(t)), \tag{4}
$$

where K_p and K_d are the control gains and x^* is the *control target*. This arrangement is primarily for convenience and ease of implementation; the methodology presented here need not be restricted in this manner. We assume that the PD controller will ensure continuous stable behaviour *provided a suitable control target is chosen*.

To continue solutions in the manner described in section 2.1 we must use the experiment to define a nonlinear function $f(x^*, \lambda)$ that is zero when the feedback-controlled experiment is tracking one of the solutions of the uncontrolled experiment. One possibility is to evaluate $x^*(t) - x(t)$ point-wise over a period; there will be zero control effort when this quantity is zero, and so x^* will be a solution of the uncontrolled experiment. (Note: measurement noise and other noise sources will mean that $x^*(t) - x(t) \approx 0$ for a solution of the uncontrolled experiment and so a suitable threshold must be chosen.)

However, x^* lives in an infinite dimensional space (for example, the space of continuously differentiable functions) and so, to realise f, we must discretize x^*. One method of discretization is to use the Fourier decomposition of x^* [Sieber and Krauskopf, 2008] and truncate to a finite (and small) number of modes. Thus, f becomes the (vector-valued) difference between the Fourier modes of the control target and the measured Fourier modes of the controlled experiment. While this is convenient theoretically, to use more than one Fourier mode results in a significant slow-down due to the extra function evaluations needed to calculate the Jacobian for the non-linear root finder. Moreover, the coupling between modes is often non-trivial and so the use of a Broyden update slows the convergence of the Newton iteration considerably.

Instead, we follow the lead of Sieber et al. [2008] and combine a single mode Fourier decomposition with time delay feedback [Pyragas, 1992, 2001]: the higher modes of the control target are provided by the delay

4

feedback. The resulting control target is given by

$$x^*(t) = \overbrace{A\sin(\omega t) + B\cos(\omega t)}^{\text{First Fourier mode of the control target}}$$

$$\underbrace{+\chi(t-T) - \left(\frac{2}{T}\int_{t-T}^{t}\chi(s)\sin(\omega s)\mathrm{d}s\right)\sin(\omega t) - \left(\frac{2}{T}\int_{t-T}^{t}\chi(s)\cos(\omega s)\mathrm{d}s\right)\cos(\omega t)}_{\text{Delay feedback with first Fourier mode removed}} \quad (5)$$

where
$$\chi(t) = Rx(t) + (1-R)\chi(t-T), \quad (6)$$

$R \in [0,1]$ is a parameter which stabilizes the delay feedback (throughout this paper $R = 0.8$), T is the period of the periodic orbit of interest and ω is the frequency of the first non-zero Fourier mode (here $\omega = \frac{2\pi}{T}$). Thus, the nonlinear function used for pseudo-arclength continuation is given by

$$f(A, B; \lambda) = \left[\begin{array}{c} A - \frac{2}{T}\int_{t-T}^{t}\sin(\omega s)x(t)\mathrm{d}s \\ B - \frac{2}{T}\int_{t-T}^{t}\cos(\omega s)x(t)\mathrm{d}s \end{array} \right] \quad (7)$$

where $x(t)$ is the measured response of the experiment. When $f(A, B; \lambda) = 0$, A and B are the first Fourier mode of the solution. To evaluate f, the (electronically controlled) parameters λ are sent to the experiment and the A and B defining the control target are sent to the real-time controller. After a suitable settling time, the first Fourier mode of the response of the experiment is measured and the value of f is computed.

With f defined in this manner, pseudo-arclength continuation may be applied directly to the experiment and, at each step, the correct values of A and B are determined by a Newton iteration.

3 Experimental rig

In this paper we present control-based continuation results from two different nonlinear devices. Both devices are energy harvesters which are designed to extract energy from vibrations in the environment: one based around an electromagnetic transducer [Barton et al., 2010] and one based around a piezoelectric beam [Stanton et al., 2010]. However, for our purposes here, we consider both devices simply as nonlinear cantilever beams with tip-masses. In both devices the nonlinearity is provided by one or more tip-mounted magnets.

3.1 Electromagnetic energy harvester

Figure 2 shows a photograph (left) and schematic (center) of the electromagnetic energy harvester and a photograph (right) of the electro-dynamic shaker. The energy harvester comprises of a iron mass and a set of neodymium (NdFeB) magnets at the tip of a spring-steel cantilever beam. The magnets are arranged with alternating polarities in the (x, y)-plane creating a closed magnetic circuit through the stator (and coil). The magnets are also arranged in the (x, z)-plane with alternating polarities to ensure that the flow of magnetic flux completely reverses direction as the beam vibrates. The magnets in combination with the iron provide a hardening spring characteristic and nonlinear damping mechanisms. When the air gap is relatively large, the system is approximately symmetric in the z-direction. However, when the air gap is reduced, asymmetries in the magnetic circuit dominate and the spring characteristics are far from symmetric.

The excitation for the energy harvester is provided by a vertically mounted electro-dynamic shaker. The shaker is displacement controlled using a proportional-integral (PI) controller implemented in analogue electronics. The input signal to the shaker is provided by a dSpace DS1104 real-time control system. The control strategy described in section 2.2 was implemented using Simulink and the Real-Time Workshop toolbox of Matlab and downloaded to the dSpace system. For feedback to the controller, the tip deflection of the energy harvester is obtained from using a suitably calibrated strain gauge (for the excitation frequencies used in this paper the beam was operating predominantly in its first bending mode).
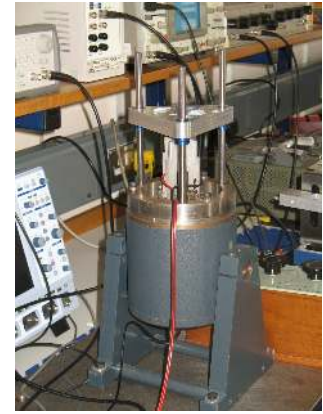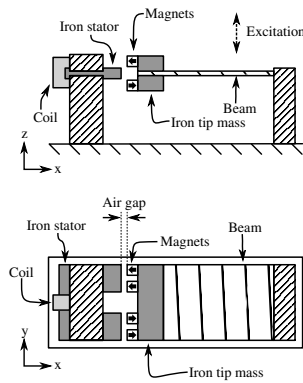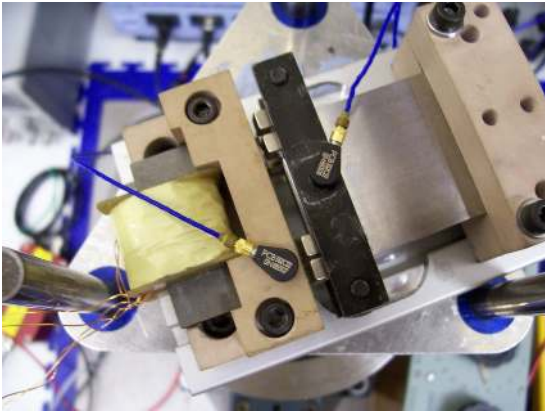
Figure 2: Left and middle: a nonlinear energy harvester using electromagnetic transduction. Right: the electro-dynamic shaker used for exciting the energy harvester. When the cantilever beam is excited in the vicinity of its natural frequency, the tip mounted magnets cause the magnetic flux through the iron cored stator to change direction thus generating a voltage across the coil. The tip mounted magnets also give rise to a nonlinear restoring force and complicated magnetic damping effects.
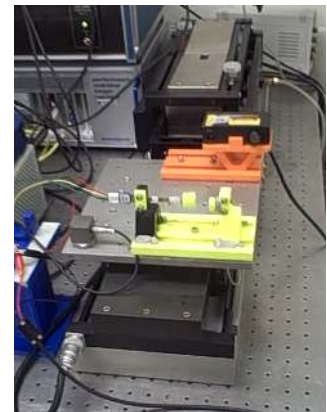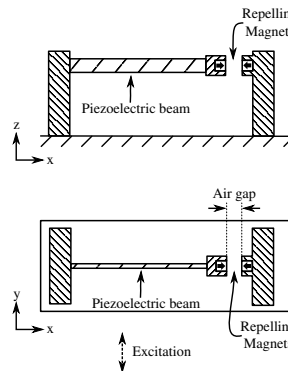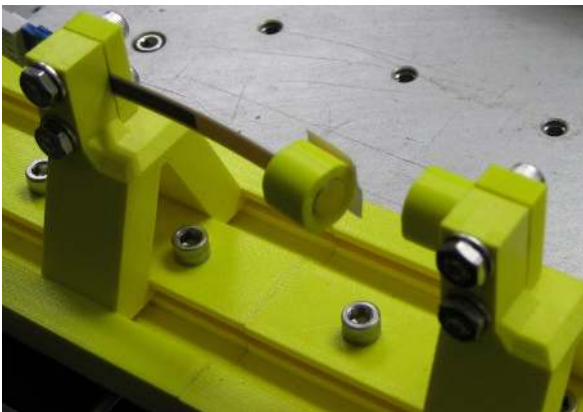

Figure 3: Left and middle: a nonlinear energy harvester based around a piezoelectric transducer. Right: the electrodynamic shaker used for exciting the energy harvester. Similar to the electromagnetic energy harvester, a tip mounted magnet provides the nonlinear restoring force; however, due to the lack of iron in the design there are minimal magnetic damping effects.

6

3.2 Piezoelectric energy harvester

Figure 3 shows a photograph (left) and schematic (center) of the piezoelectric energy harvester and a photograph (right) of the electro-dynamic shaker. The energy harvester comprises of a cantilevered bimorph piezoelectric beam (V22BL, Midé Corporation) with a cylindrical neodymium (NdFeB) magnet at the tip. For the purpose of the experiments here, the piezoelectric laminates (PZT-5H) are not connected. The tip magnet is positioned in line with a second magnet rigidly attached to the base of the harvester such that the two magnets repel each other. In this configuration the spring characteristic of the harvester is softening, and for a sufficiently small air gap between the magnets the harvester is bistable. Similar to the electromagnetic energy harvester, for small air gaps the asymmetries between the magnets dominate the nonlinear spring characteristics. However, since there is no iron present, there is negligible nonlinear damping (i.e., linear viscous damping provides a good approximation to the physics).

The excitation for the energy harvester is provided by a horizontally mounted electro-dynamic shaker (APS 129a long stroke shaker with air bearings) used in controlled-current mode. The input signal to the shaker is provided by a SpeedGoat Performance Real-Time Target machine. As with the electromagnetic harvester, the control strategy described in section 2.2 was implemented using Simulink and the Real-Time Workshop toolbox of Matlab and downloaded to the target machine. To measure the tip displacement of the cantilever beam, a laser displacement sensor, a Microepsilon model LD 1605, was used, the output of which was fed directly into the target machine.

4 Results

In this section, we present the experimental results for both energy harvesters using control-based continuation. Each harvester is excited with sinusoidal forcing close to the respective resonant frequency. In each case the experimental results are compared with a semi-static frequency sweep of the system. For a qualitative comparison, we begin by providing theoretical results using a harmonic balance solution of the Duffing equation, which can be considered a first-order approximation of the true models.

4.1 Theoretical results

The simplest, non-trivial model for the energy harvesting devices considered in this paper is the single degree-of-freedom Duffing equation:

$$m\ddot{x} + c\dot{x} + \alpha k x + \beta k_3 x^3 = f\cos(\Omega t), \tag{8}$$

where m is the mass, c represents the combined effect of mechanical and electrical dissipation, $\alpha k x + \beta k_3 x^3$ represents the restoring force, and $f\cos\Omega t$ is a harmonic base excitation of acceleration amplitude f and frequency Ω. The coefficients α and β can take the values ± 1 and so determine whether the restoring force is hardening, softening or bistable. Equation (8) fails quantitatively in its reproduction of the behaviour of the physical devices, however, it features all of the qualitative features seen experimentally.

Equation (8) can be non-dimensionalized by introducing a dimensionless displacement $y = x/\ell$ and time $\tau = t\sqrt{k/m}$, where and $\ell^2 = k/k_3$; the corresponding dimensionless equation is

$$y'' + \mu y' + \alpha y + \beta y^3 = \Gamma\cos(\eta\tau) \tag{9}$$

where $()'$ denotes a derivative with respect to dimensionless time, μ is the dimensionless damping coefficient, $\Gamma = f\sqrt{k_3/k^3}$ is a dimensionless excitation term, and $\eta = \Omega\sqrt{m/k}$ provides a dimensionless frequency. If we assume a solution in the form of a truncated Fourier series with coefficients that slowly vary with time $y = p(\tau) + a(\tau)\cos(\eta\tau) + b(\tau)\sin(\eta\tau)$, the first and second derivatives become

$$y' = p' + (a' + b\eta)\cos(\eta\tau) + (b' - a\eta)\sin(\eta\tau), \tag{10a}$$

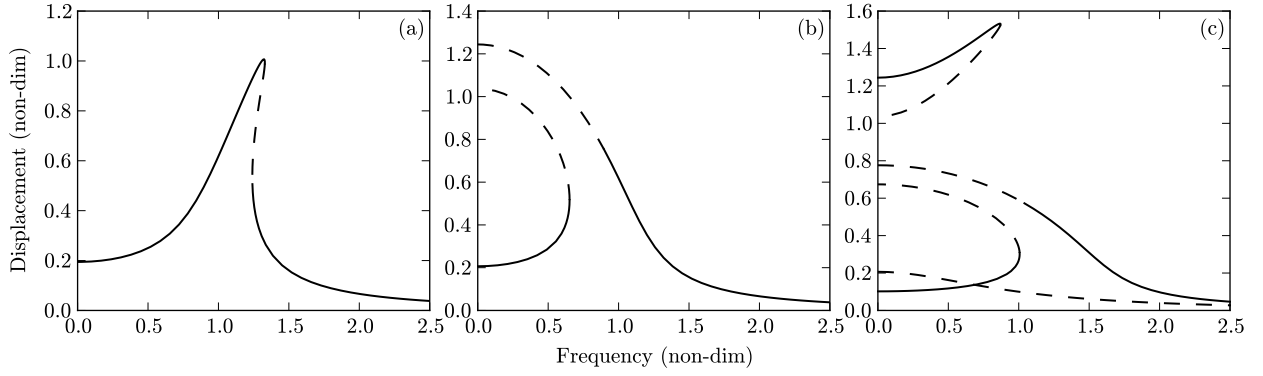$$y'' = p'' + (2b' - a\eta)\eta\cos(\eta\tau) + (b\eta - 2a')\eta\sin(\eta\tau), \tag{10b}$$

Figure 4: Panels (a), (b) and (c) show the frequency response function of the Duffing equation (9) in hardening, softening and bistable configurations respectively. Stable solution branches are denoted with a solid curve and unstable solution branches are denoted with a dashed curve. For each panel $\mu = 0.15$ and $\Gamma = 0.2$.

where we have presumed that $p'' = a'' = b'' = 0$ owing to the slowly varying approximation. The expressions for y, y', and y'' are then substituted into (9) and the constant coefficients, along with the coefficients of $\cos(\eta\tau)$ and $\sin(\eta\tau)$, are balanced on each side. Balancing the constant coefficients gives

$$\mu p' = -p \left(\beta p^2 + \alpha + \frac{3}{2}\beta r^2 \right),$$ (11)

and balancing the coefficients of $\cos(\eta\tau)$ and $\sin(\eta\tau)$ gives

$$\begin{pmatrix} \mu & 2\eta \\ -2\eta & \mu \end{pmatrix} \begin{pmatrix} a' \\ b' \end{pmatrix} = \begin{pmatrix} a \left(\eta^2 - \alpha - 3\beta p^2 - \frac{3}{4}\beta r^2 \right) - \mu\eta b + \Gamma \\ b \left(\eta^2 - \alpha - 3\beta p^2 - \frac{3}{4}\beta r^2 \right) + \mu\eta a \end{pmatrix},$$ (12)

where $r^2 = a^2 + b^2$. The steady-state response, $\tilde{p}$, $\tilde{r}$, is obtained from the fixed points of (11) and (12), which requires $a' = b' = p' = 0$; squaring and summing the result from (12) gives the frequency response equation

$$\left[\left(\eta^2 + \alpha - 3\beta\tilde{p}^2 - \frac{3}{4}\beta\tilde{r}^2 \right)^2 + (\mu\eta)^2 \right] \tilde{r}^2 = \Gamma^2$$ (13)

where $\tilde{p}$ may take on multiple values. More specifically, after setting $p' = 0$ in (11), the steady-state solution $\tilde{p}$ reveals that both $\tilde{p} = 0$ and $\tilde{p}^2 = -\alpha/\beta - \frac{3}{2}\tilde{r}^2$ are fixed points. In the bistable case, where $\alpha = -1$ and $\beta = 1$, the latter solution is interesting because it restricts the values of $\tilde{r}$ that provide a physical solution for $\tilde{p}$ to $\tilde{r}^2 \leq \frac{2}{3}$.

Figure 4 shows the solutions of (13) for the cases of hardening ($\alpha = +1$, $\beta = +1$), softening ($\alpha = +1$, $\beta = -1$) and bistable ($\alpha = -1$, $\beta = +1$) springs as the dimensionless parameter η is varied. Both Γ and μ are fixed at 0.2 and 0.15 respectively. In all three cases there are coexisting solutions around the resonance peak due to the 'bending over' of the frequency response curve. In addition, there exists a high-amplitude, low-frequency branch of solutions for the bistable case. Note that in the softening case there exist unbounded solutions due to the $-y^3$ term; in the physical system there exist higher-order nonlinearities which bound the solutions and result in a frequency response much more like a reflection of the hardening frequency response.

4.2 Hardening and softening spring characteristics

Figure 5 shows an initial forwards and backwards frequency sweep (marked with crosses), without feedback control, of the electromagnetic energy harvester in its hardening spring configuration. The presence of a hysteresis loop is clear; between 17.15 Hz and 25.35 Hz there exist two stable periodic solutions, one high amplitude and one low amplitude.
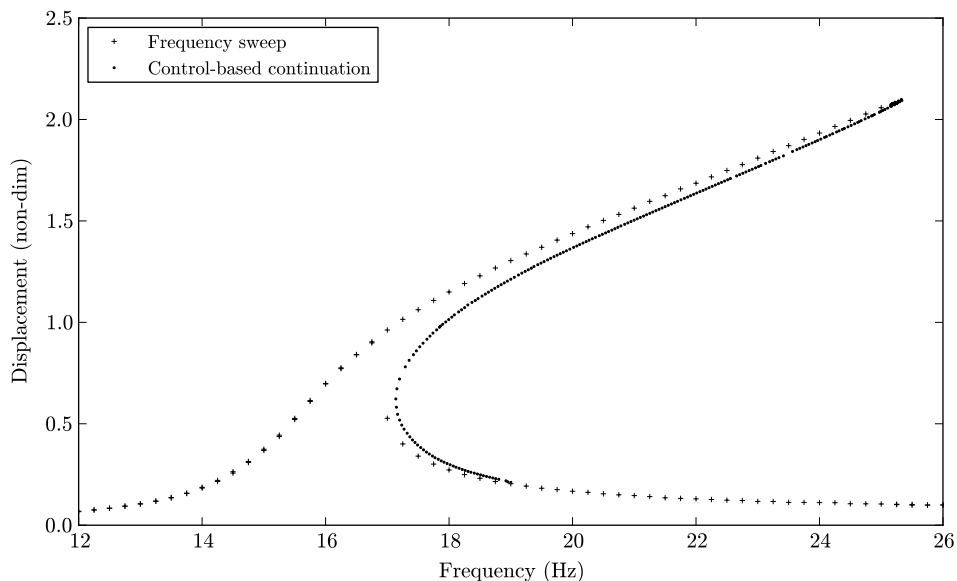
Figure 5: Experimental results for the electromagnetic energy harvester in a hardening spring configuration. The results of a forwards and backwards frequency sweep are marked with crosses and the results of a control-based continuation run starting at 19 Hz are marked with dots.

A control-based continuation run was started from two stable, small amplitude solutions at 19 Hz and 18.95 Hz respectively. (Two initial solutions are required in order to calculate a secant for the prediction step.) As the continuation run (marked with dots in figure 5) progressed, the excitation frequency decreased towards a fold/saddle-node bifurcation at 17.15 Hz. With the use of the pseudo-arclength equation in the nonlinear problem formulation, the continuation run was able to pass through the first fold and track up the branch of unstable solutions towards the second fold at the resonance peak. The continuation run was stopped shortly after passing through the second fold onto the branch of stable, large amplitude solutions. Note: the sharpness of the resonance peak is primarily due to the projection onto the amplitude-frequency plane; when viewed in the full state-space, the solution curve is smooth. A qualitative comparison of figure 5 and figure 4(a) shows good agreement.

Throughout the continuation run, the step size remained approximately constant (although this is not clear from figure 5. This gave a good distribution of data points, even in the vicinity of the folds. We note that there is a small discrepancy between the control-based continuation run and the frequency sweep; this occurs with both experimental rigs and so we leave discussion of this phenomenon until section 5.

Experimental results for the piezoelectric energy harvester in a softening spring configuration are shown in figure 6. As with the electromagnetic harvester, an initial forward and backward frequency sweep was performed which revealed a hysteresis loop between 7.6 Hz and 9.25 Hz; again there exists a high amplitude solution and a low amplitude solution.

A control-based continuation run was started from two stable low-amplitude solutions at 9 Hz and 9.05 Hz respectively. The continuation run passed through the fold at 9.25 Hz and tracked up the branch of unstable solutions. At approximately 8.7 Hz, the settling time of the PD controller had increased unacceptably and so the control gains were increased at that point. After that no further control-related problems were encountered.

As with the hardening case, the control-based continuation resulted in a good distribution of solution points without large gaps. However, there was a noticeable discrepancy between the frequency sweep and the continuation results at the resonance peak.

As noted in section 4.1, there is a qualitative difference between the results shown in figure 4(b) and the results shown in figure 6. This is due to the presence of higher-order nonlinearities which prevent the upper solution branch from becoming unstable.
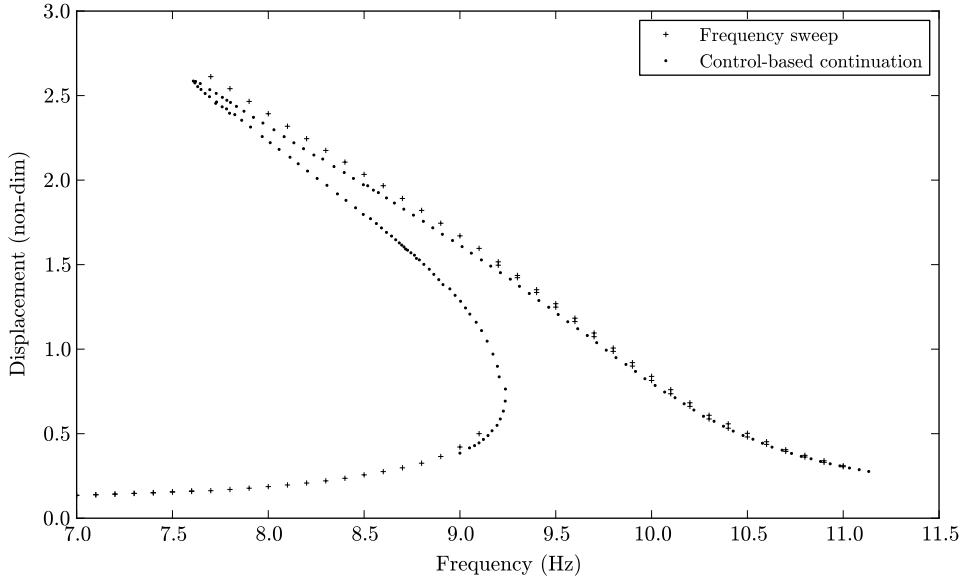
Figure 6: Experimental results from the piezoelectric energy harvester in a softening spring configuration. The results of a forwards and backwards frequency sweep are marked with crosses and the results of a control-based continuation run starting at 9 Hz are marked with dots.

4.3 Bistable spring characteristics

After investigating the piezoelectric energy harvester in its softening configuration, the length of the cantilever beam was adjusted such that the magnetic forces gave rise to a bistable configuration. We note that in this configuration the device was particularly sensitive to disturbances due to difficulties in maintaining the magnets in a fixed alignment.

As an initial investigation, a series of low-amplitude frequency sweeps were performed such that the motion of the harvester remained entirely within one of the potential wells. Further to this, continuation runs were performed at the same amplitude levels, as shown in figure 7 thus demonstrating that continuation runs can be performed semi-automatically (i.e., once programmed through Matlab, all of the continuation runs proceeded sequentially without user intervention).

For the experimental results shown in figure 8, the amplitude of excitation was increased so that large amplitude, cross-well solutions existed. Two continuation runs were attempted; one along the branch of large amplitude, cross-well solutions and one along the resonance branch emanating from one of the potential wells. The comparison with the theoretical results in figure 4(c) is striking; there is excellent qualitative agreement. Example solutions from the large amplitude, cross-well solution branch are shown in figure 9 which show the phase difference between the stable and unstable solutions.

Along the resonance branch shown in figure 8, both the frequency sweep and the continuation run end abruptly. Careful analysis of the frequency sweep shows a period doubling bifurcation just before the branch ends; immediately after the period doubling bifurcation (within 0.05 Hz) transient chaos is seen before the solution collapses onto the low amplitude solution branch. The reason for the failure of the continuation run is due to the failure of the PD controller; at that point it exhibited extreme sensitivity to the choice of control gains, suggesting a more sophisticated feedback controller is needed.

As a final test of the control-based continuation technique, a series of continuation runs were started from the high-amplitude cross-well solution branch, decreasing the excitation amplitude; the results are shown in figure 10 where the curves shown are a quartic polynomial least-squares fit to the data. As expected, the continuation runs showed the existence of series of folds; should the excitation amplitude be decreased below the folds, the branch of high-amplitude cross-well solutions will cease to exist.
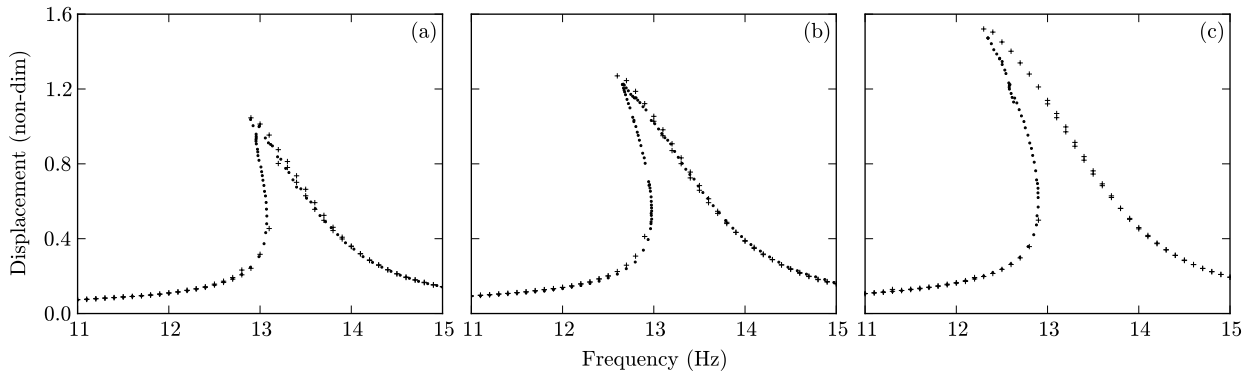
Figure 7: A sequence of experimental results for the piezoelectric energy harvester in its bistable configuration; each shows a frequency sweep marked with crosses and a continuation run marked with dots. In each plot the harvester was excited with a constant amplitude sinusoid with the electrodynamic shaker in current mode (thus corresponding to a constant acceleration amplitude frequency sweep). The amplitude of excitation was kept sufficiently low to ensure that the motion of the harvester remained inside one of the potential wells.
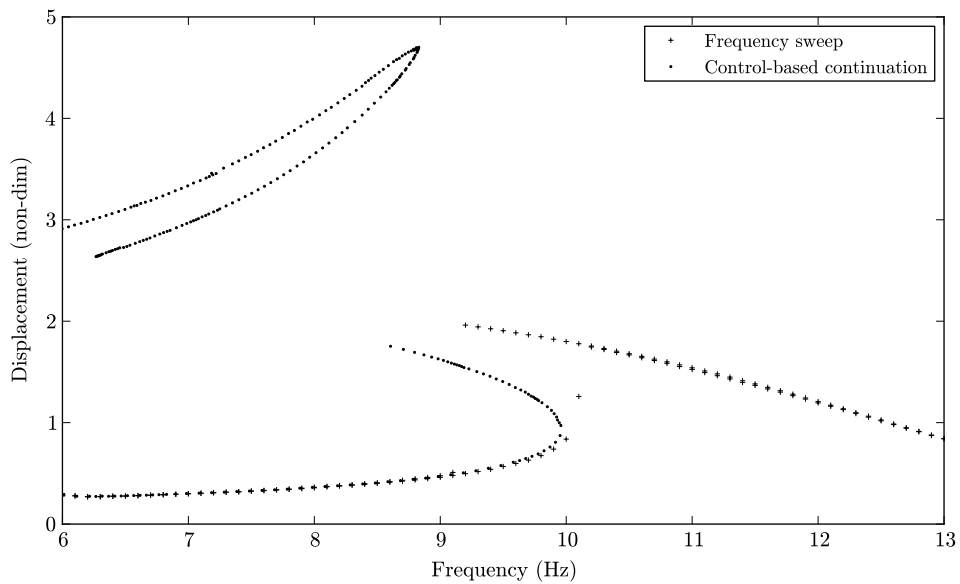

Figure 8: Experimental results from the piezoelectric energy harvester in its bistable configuration. The harvester was excited with high-amplitude forcing, thus ensuring the existence of a high amplitude, cross-well solution branch (cf., figure 4(c)).
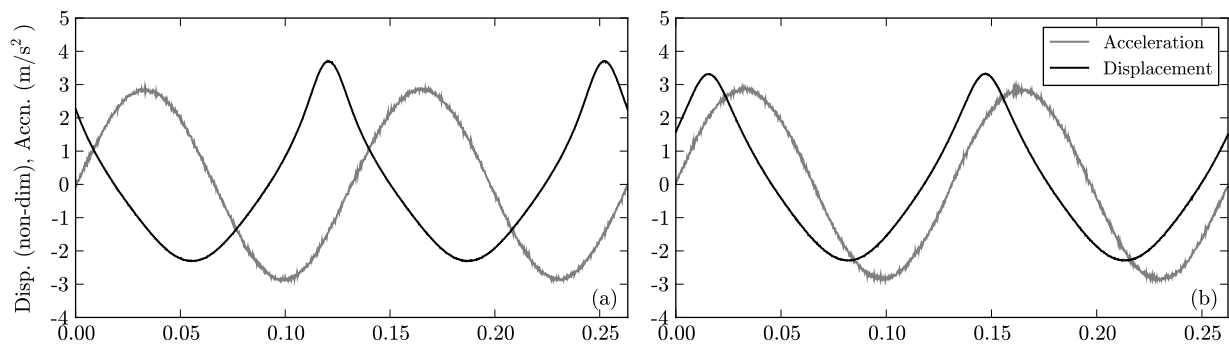
Figure 9: Two solution profiles for the bistable piezoelectric energy harvester oscillating at 7.6 Hz taken from the results shown in figure 8. The left-hand panel shows the stable solution and the right-hand panel shows the coexisting unstable solution.
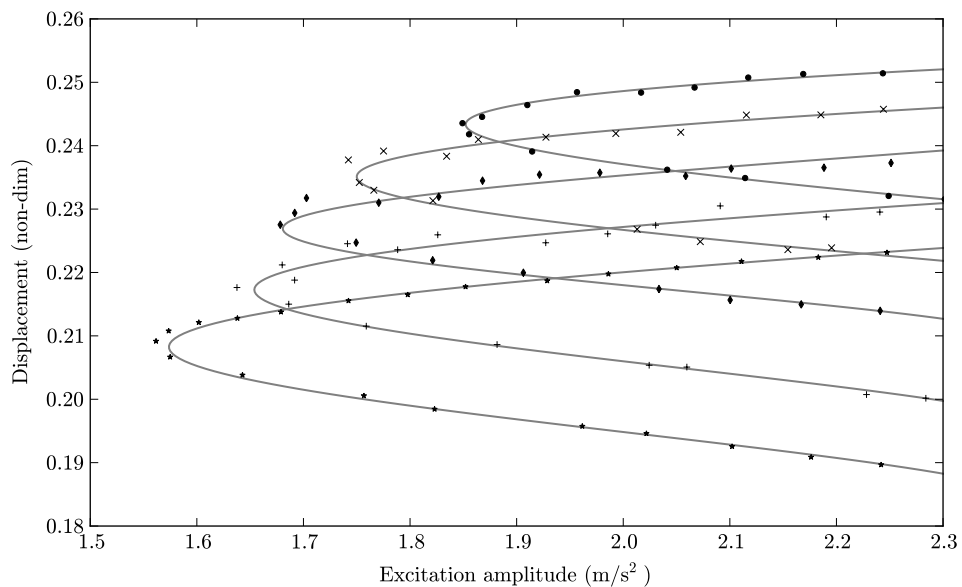

Figure 10: A series of continuation runs that vary the amplitude of excitation through a fold. Each continuation run starts on the stable branch of high-amplitude cross-well solutions shown in figure 8.

5 Discussion and conclusions

As mentioned in the previous section, there is a small discrepancy between the initial frequency sweeps performed on each of the experiments and the subsequent continuation runs. There are several possible causes for this:

Invasive control scheme Inevitably there is measurement noise in the control loop which prevents the controller from being completely non-invasive. In particular, when the control gains are high there may be a large high-frequency component to the feedback signal. In this context the work presented here is reminisent of the work of Barkley et al. [2006] which considers the application of coarse-graining techniques to the numerical continuation of stochastic ordinary differential equations. In that work, the difference in the resulting bifurcation diagram due to noise is clear. It is unlikely that this source of error will ever be removed and can only be minimised through the use of high-quality measurement equipment and other noise reduction methods (e.g., filtering).

Experimental creep The cantilever beams in both the experiments were strongly clamped. However, due to the nature of the materials involved, there is the possibility for small amounts of creep in the mounting of the cantilever beam and the tip magnets. As such, the experiments become time-varying and the repeatability, which is paramount for control-based continuation, becomes poor. The only way to remedy this problem is to design and build high-quality experiments.

Large tolerances The tolerances for the nonlinear root finder where largely empirically determined and, consequently, they may have been sub-optimal. The larger the tolerance, the more uncertainty there is in the exact location of the solution in phase-space; this uncertainty then propagates through to the bifurcation diagram. Ideally, confidence intervals would be calculated for the computed bifurcation diagrams. The minimum tolerances are determined by the levels of measurement noise in the system and the amount of time required to evaluate the nonlinear function (7) (i.e., if the time to evaluate is large then a larger tolerance is used to reduce the overall experimentation time).

In general, the discrepancies between the initial frequency sweeps and the continuation runs are very small which suggests that the results from the control-based continuation are reliable. As such, the systematic study presented here demonstrates that the control-based continuation method can be extremely useful in determining the bifurcation structure of a physical experiment without the use of a mathematical model. While in these particular experiments, knowledge of the unstable solutions does not add significantly to our overall knowledge of the system, there are many systems where knowledge of the unstable orbits may be extremely valuable, for example, where the unstable solutions act as a separatrix between other stable solutions.

In the future, we hope to extend this work to the continuation of bifurcations in two (or more) parameters. For example, the tracking of saddle-node bifurcations (folds) is a standard task in numerical continuation; if it is possible to do this in control-based continuation it will enable stability boundaries to be tracked directly in an experiment. In order to do this it will be necessary to develop suitable bifurcation test functions (functions that are zero at the bifurcation points and no-where else). The current test functions used in numerical continuation are not suitable due to their reliance on derivative information which is typically highly inaccurate when estimated from measured data.

One of the remaining difficulties in control-based continuation is the construction of a suitable controller for the overall system (once the control target has been establised). While a simple proportional-derivative controller has been used here, it would be extremely beneficial to use an adaptive/updateable control scheme to ensure stable operation regardless of the nonlinearities present. Since the overall predictor-corrector nature of the continuation algorithm ensures that only small steps are taken in the system parameters and phase-space, it should be possible to develop a widely applicable controller that incorporates information from the continuation run as it progresses.

6 Acknowledgements

References

D. Barkley, I.G. Kevrekidis, and A.M. Stuart. The moment map: nonlinear dynamics of density evolution via a few moments. *SIAM Journal on Applied Dynamical Systems*, 5(3):403–434, 2006.

D.A.W. Barton and S.G. Burrow. Numerical continuation in a physical experiment: investigation of a nonlinear energy harvester. In *ASME 2009 International Design Engineering Technical Conferences*, San Diego, USA, 30th August–2nd September 2009.

D.A.W. Barton, S.G. Burrow, and L.R. Clare. Energy harvesting from vibrations with a nonlinear oscillator. *ASME Journal of Vibrations and Acoustics*, 132(2):021009, 2010.

M. Breakspear, J.A. Roberts, J.R. Terry, S. Rodrigues, N. Mahant, and P.A. Robinson. A unifying explanation of primary generalized seizures through nonlinear brain modeling and bifurcation analysis. *Cerebral Cortex*, 16 (9):1296–1313, 2006.

E.J. Doedel, H.B. Keller, and J.P. Kernevez. Numerical analysis and control of bifurcation problems, part I. *International Journal of Bifurcation and Chaos*, 1(3):493–520, 1991a.

E.J. Doedel, H.B. Keller, and J.P. Kernevez. Numerical analysis and control of bifurcation problems, part II. *International Journal of Bifurcation and Chaos*, 1(4):745–772, 1991b.

V. Eyert. A comparative study on methods for convergence acceleration of iterative vector sequences. *Journal of Computational Physics*, 124(15):271–285, 1996.

B. Krauskopf. *Unlocking dynamical diversity: optical feedback effects on semiconductor lasers*, chapter Bifurcation analysis of lasers with delay, pages 147–183. Wiley, New Jersey, 2005.

B. Krauskopf, H. Osinga, and J. Galán-Vioque, editors. *Numerical continuation methods for dynamical systems: path following and boundary value problems*, chapter Lecture notes on numerical analysis of nonlinear equations, pages 1–49. Springer-Verlag, Dordrecht, The Netherlands, 2007.

B.P. Mann and B.A. Owens. Investigations of a nonlinear energy harvester with a bistable potential well. *Journal of Sound and Vibration*, 329(9):1215–1226, 2010.

B.P. Mann and N.D. Sims. Energy harvesting from the nonlinear oscillations of magnetic levitation. *Journal of Sound and Vibration*, 319(1–2):515–530, 2009.

S. Misra, H. Dankowicz, and M.R. Paul. Event-driven feedback tracking and control of tapping-mode atomic force microscopy. *Proceedings of the Royal Society A*, 2008.

F.C. Moon and P.J. Holmes. A magnetoelastic strange attractor. *Journal of Sound and Vibration*, 65(2):275–296, 1979.

A.H. Nayfeh. *Perturbation methods*. Wiley, 2000.

E. Ott, C. Grebogi, and J.A. Yorke. Controlling chaos. *Physical Review Letters*, 64(11):1196–1199, 1990.

K. Pyragas. Continuous control of chaos by self-controlling feedback. *Physics Letters A*, 170(6):421–428, November 1992.

K. Pyragas. Control of chaos via an unstable delayed feedback controller. *Physical Review Letters*, 86(11):2265–2268, Mar 2001.

R. Seydel. *Practical bifurcation and stability analysis*, volume 5 of *Interdisciplinary Applied Mathematics*. Springer, New York, 3rd edition edition, 2010.

J. Sieber and B. Krauskopf. Control based bifurcation analysis for experiments. *Nonlinear Dynamics*, 51(3):365–377, 2008.

J. Sieber, A. Gonzalez-Buelga, S.A. Neild, D.J. Wagg, and B. Krauskopf. Experimental continuation of periodic orbits through a fold. *Physical Review Letters*, 100(24):244101, 2008.

C.I. Siettos, I.G. Kevrekidis, and D. Maroudas. Coarse bifurcation diagrams via microscopic simulators: a state-feedback control-based approach. *International Journal of Bifurcation and Chaos*, 14(1):207–220, 2004.

S.C. Stanton, C.C. McGehee, and B.P. Mann. Reversible hysteresis for broadband magnetopiezoelastic energy harvesting. *Applied Physics Letters*, 95(17):174103, 2009.

S.C. Stanton, C.C. McGehee, and B.P. Mann. Nonlinear dynamics for broadband energy harvesting: Investigation of a bistable piezoelectric inertial generator. *Physica D*, 239(10):640–653, 2010.

G. Stépán. Modelling nonlinear regenerative effects in metal cutting. *Philosophical Transactions of the Royal Society*, 359(1781):739–757, 2001.

A. Triplett and D.D. Quinn. The effect of non-linear piezoelectric coupling on vibration-based energy harvesting. *Journal of Intelligent Material Systems and Structures*, 20(16):1959–1967, 2009.